12. Callahan AP, Rice DE, Knapp FF Jr. Availability of Re-188 from a tungsten-188/Re188 generator system for therapeutic applications [Abstract]. *J Nucl Med* 1987;28:657.
13. Callahan AP, Rice DE, Knapp FF Jr. Rhenium-188 for therapeutic applications from an alumna based tungsten-188/Re-188 radionuclide generator. *Nucl Compact Eur Am Commun Nucl Med* 1989;20:3–6.
14. Ehrhardt G, Ketring AP, Turpin TA, Razavi MS, Vanderherden J-L, Fritzberg AR. An improved tungsten-188/Re-188 generator for radiotherapeutic application. *J Nucl Med* 1987;28:656–657.
15. Kirschner A, Ice R, Beierwaltes W. Radiation dosimetry of ^{131}I-19-iodocholesterol: the pitfalls of using tissue concentration data: the author's reply. *J Nucl Med* 1975;16:248–249.
16. Loevinger R, Budinger T, Watson E. *MIRD primer for absorbed dose calculation.* New York: Society of Nuclear Medicine, 1988.
17. Cloutier R, Smith S, Watson E, Snyder W, Warger G. Dose to the fetus from radionuclides in the bladder. *Health Phys* 1973;25:147–161.
18. Stabin MG. MIRDOSE. Personal computer software for internal dose assessment in nuclear medicine. *J Nucl Med* 1996;37:538–546.
19. Culter SJ, Ederer F. Maximum utilization of the life table method in analyzing survival. *J Chronic Dis* 1958;8:699–712.
20. Breslow N. A generalized Kruskal-Wallis test for comparing K samples subject to unequal patterns of censorship. *Biometrika* 1970;57:579–594.
21. Park CH, Sub JH, Yoo HS, Lee JT, Kim DI. Evaluation of intrahepatic ^{131}I-ethiodol on a patient with hepatocellular carcinoma: therapeutic feasibility study. *Clin Nucl Med* 1986;11:514–517.
22. Fox RA, Klemp PF, Egan G, Mina LL, Burton MA, Gray BN. Dose distribution following selective internal radiation therapy. *Int J Radiat Oncol Biol Phys* 1991;21:463–467.
23. Callahan AP, Rice DE, Knapp FF Jr. Availability of rhenium-188 from a tungsten-188/Re188 generator system for therapeutic applications [Abstract]. *J Nucl Med* 1987;28:657p.
24. Mantravadi RVP, Spigos DG, Karesh SM. Intra-arterial P-32 Chromic phosphate for the prevention of postoperative liver metastases in high risk colorectal cancer patients. *Radiology* 1983;148:555–559.
25. Ho S, Lau WY, Leung WT. Ultrasound guided internal radiotherapy using yttrium-90 glass microspheres for liver malignancies [Letter]. *J Nucl Med* 1997;38:1169.

Carbon-11-Thymidine and FDG to Measure Therapy Response

Anthony F. Shields, David A. Mankoff, Jeanne M. Link, Michael M. Graham, Janet F. Eary, Susie M. Kozawa, Minna Zheng, Barbara Lewellen, Thomas K. Lewellen, John R. Grierson and Kenneth A. Krohn

Departments of Medicine and Radiology, Karmanos Cancer Institute, Wayne State University, Detroit, Michigan; and Department of Radiology, Imaging Research Laboratory, University of Washington, Seattle, Washington

This study was performed to determine if PET imaging with ^{11}C-thymidine could measure tumor response to chemotherapy early after the initiation of treatment. Imaging of deoxyriboneucleic acid biosynthesis, quantitated with ^{11}C-thymidine, was compared with measurements of tumor energetics, obtained by imaging with ^{18}F-fluorodeoxyglucose (FDG). **Methods:** We imaged four patients with small cell lung cancer and two with high-grade sarcoma both before and approximately 1 wk after the start of chemotherapy. Thymidine and FDG studies were done on the same day. Tumor uptake was quantified by standardized uptake values (SUVs) for both tracers by the metabolic rate of FDG and thymidine flux constant (K_{TdR}) using regions of interest placed on the most active part of the tumor. **Results:** In the four patients with clinical response to treatment, both thymidine and FDG uptake markedly declined 1 wk after therapy. Thymidine measurements of SUV and K_{TdR} declined by 64% ± 15% and 84% ± 33%, respectively. FDG SUV and the metabolic rate of FDG declined by 51% ± 9% and 63% ± 23%, respectively. In the patient with metastatic small cell lung cancer who had disease progression, the thymidine SUV decreased by only 8% (FDG not done). In a patient with abdominal sarcoma and progressive disease, thymidine SUV was essentially unchanged (declined by 3%), whereas FDG SUV increased by 69%. **Conclusion:** Images show a decline in both cellular energetics and proliferative rate after successful chemotherapy. In the two patients with progressive disease, thymidine uptake was unchanged 1 wk after therapy. In our limited series, K_{TdR} measurements showed a complete shutdown in tumor proliferation in patients in whom FDG showed a more limited decrease in glucose metabolism.

Key Words: PET; thymidine; fluorodeoxyglucose

J Nucl Med 1998; 39:1757–1762

PET provides a way of measuring regional tumor metabolism and the response to therapy. At present, clinicians use techniques that measure the change in size of a tumor to determine if it is responding to chemotherapy. Because tumor shrinkage is often delayed after successful cytotoxic therapy, anatomic imaging is typically repeated after at least 2 mo of therapy. Even then, persistence of fibrotic or inflammatory masses may make it difficult to judge true tumor response to treatment. PET can aid in this task, because metabolic changes in the tumor are expected to precede changes in size. As PET is being developed for tumor imaging, among the major issues to be addressed are the optimal imaging agent to be used and the timing of imaging. Fluorodeoxyglucose (FDG) has been the most widely used agent in PET tumor imaging. This stems in part from its relatively straightforward synthesis, long half-life for a PET radionuclide (110 min) and high tumor uptake. FDG may encounter problems in some situations in which tumor cells may continue to be energetically active even after their replicative machinery has been damaged. Furthermore, FDG may be taken up by inflammatory cells such as macrophages found in dying tumors (*1*). We have, therefore, sought to study tracers that may be more closely tied to cellular proliferation (*2,3*).

Because thymidine is readily taken up by cells and incorporated into deoxyriboneucleic acid (DNA), it has been used for many years to assess cell growth when labeled with long-lived tracers such as ^{14}C and ^{3}H. Studies in rats have shown that DNA and protein biosynthesis decline after therapy more promptly than FDG uptake (*4*). We have been studying ^{11}C-thymidine kinetics compared with FDG in patients undergoing chemotherapy. The ability to label thymidine with ^{11}C allows the production of images of uptake and retention (*5,6*). In patients with lymphoma, ^{11}C-thymidine uptake correlated with tumor grade (*7*). Carbon-11-thymidine can be produced for PET imaging with the label in either the methyl or ring-2 positions. The ring-2 form of thymidine was chosen because it is primarily degraded to CO_2, which simplifies its quantitation and modeling (*8,9*). In this study, we examined the changes seen in thymidine uptake early after the onset of chemotherapy in patients with small cell lung cancer and sarcoma. This study

Received Sept. 2, 1997; revision accepted Dec. 24, 1997.
For correspondence or reprints contact: Anthony F. Shields, MD, PhD, Harper Hospital, 534 Hudson, 3990 John R St., Detroit, MI 48301.

was designed to determine if very early changes in DNA synthesis would be useful in assessing treatment response.

MATERIALS AND METHODS

Patients

We evaluated six patients (6 men; age range 45–69 yr; mean age 60 yr), four with small cell lung cancer and two with sarcomas. Cancer was newly diagnosed in all patients, and none had received prior chemotherapy. The patients with small cell lung cancer all had extensive disease and received chemotherapy with cisplatin on Day 1 and etoposide for 3 days. One patient (Patient 5) had a high-grade sarcoma in his thigh with pulmonary metastases and was treated with MAID [mesna, doxorubicin (Adriamycin), ifosfamide and dacarbazine] chemotherapy (*10*). In the patient who had an abdominal sarcoma, after initial surgical resection, it rapidly recurred, and he was treated with Adriamycin and dacarbazine. Patients were studied just before chemotherapy and again approximately 1 wk after chemotherapy started (mean 7.7 days; range 6–11 days). Although some patients had responses to chemotherapy, all patients subsequently died from either progressive or recurrent disease. All imaging study protocols were approved by institutional Human Subject and Radiation Safety Committees, and all patients gave informed consent.

At the time of imaging, all patients were in good overall health other than the presence of their cancers. All patients underwent blood tests to determine hematocrit, white blood cell counts and platelet counts before each study. All patients had hematocrits greater than 30% and platelet counts greater than 150,000/μl. No patient was neutropenic. All patients had renal and hepatic function within normal limits. All patients were interviewed, and blood pressure and pulse measurements were taken on the day of the study to ensure that patients were reasonably hydrated, especially after chemotherapy. All patients fasted overnight before the study and had plasma glucose measurements taken as part of the study. One patient (Patient 3) had noninsulin-dependent diabetes mellitus and required 5 U of regular insulin to bring his plasma glucose to less than 130 mg/dl in his baseline but not post-therapy study. None of the remaining patients had evidence of glucose intolerance.

Radiochemistry

Carbon-11-thymidine labeled in the ring-2 position was prepared just before use according to a modification of the method of Vander Borght et al. (*6*) and Link et al. (*11*). The radiochemical purity of high-performance liquid chromatography (HPLC) isolated material was >96%, except in one patient in which it was 85%. The activity of ^{11}C-thymidine injected ranged from 128 to 819 MBq (3.5–22.1 mCi, mean 550 MBq), and the specific activity was 0.27–61.5 GBq/μmol (mean 15 GBq/μmol) at the time of injection. FDG was synthesized by the method of Hamacher et al. (*12*). Radiochemical purity and specific activity were measured by HPLC using an aminopropyl/normal phase column eluated with acetonitrile/water and followed by radiation and refraction index detectors. The amount of FDG injected ranged from 284 to 401 MBq (7.7–10.8 mCi, mean 350 MBq) and had a purity of >97% and specific activity of >47 GBq/mmol at the time of injection.

PET Imaging and Data Analysis

Patients fasted overnight before the study but were allowed noncaloric liquids. Thirty-minute transmission studies, obtained for attenuation correction, were obtained before tracer injection. In all patients, dynamic PET imaging was performed with each tracer, starting at the beginning of a 1-min infusion of thymidine or a 2-min infusion of FDG. Timing of the dynamic imaging studies was as follows: 4 × 20-sec scans, 4 × 40-sec scans, 4 × 1-min scans, 4 × 3-min scans and 8 × 5-min scans. Two patients were imaged on an SP-3000 tomography unit (PET Electronics, St. Louis, MO) with four imaging planes (plane thickness 11.5 mm, with a 3.5-mm gap between planes) (*13,14*). Four patients were imaged on an Advance tomography unit (GE Medical Systems, Milwaukee, WI) operating in high-sensitivity mode with 35 imaging planes (plane thickness 4.25 mm without a gap) (*15,16*). All images were corrected for scattered and random coincidences.

To obtain tissue time-activity curves, region-of-interest (ROI) analysis was performed on the dynamic images. ROIs were drawn using both the summed 20–60-min thymidine and 30–60-min FDG images combined with CT or MR images as guides. The same ROIs were used to analyze the thymidine and FDG studies done on the same day. ROIs were drawn over the portion of the tumor containing maximal counts on the summed images. On SP-3000 images, a 9–19-mm-diameter ROI was placed on a single plane. On the Advance tomograph, which had a thinner plane, a 19-mm-diameter ROI was placed in the three adjacent image planes with maximal tumor counts, and counts from the three planes were summed for each time bin. On all studies, the site of maximal tumor counts on the thymidine image was within several pixels of the maximal tumor site on FDG summed images. On post-therapy studies, tumor sites could not always be identified on thymidine images, in which case only the FDG images were used to draw ROIs. The same size ROI was used on both pre- and post-therapy studies. Because ROIs were drawn in the center of relatively large tumors, no partial-volume correction was warranted. Tissue and blood time-activity curves were decay corrected and converted to μCi/ml units using calibration data obtained at the time of each study.

To obtain the input function for the amount of thymidine delivered to the tumor through the bloodstream, we obtained arterial or venous blood samples when possible. These blood samples were then analyzed to determine the total activity in whole blood as a function of time and the fraction of activity in intact thymidine versus labeled metabolites (*9*). Briefly, an aliquot of each sample was mixed with NaOH to retain radiolabeled CO_2 and bicarbonate and thereby measure total activity. Selected samples underwent treatment with acid to remove labeled CO_2/HCO_3^- and to measure these species (CO_2) by difference with the total blood activity. Samples were also analyzed by HPLC to determine the fraction of non-CO_2 activity present as intact thymidine versus thymine or related small molecules (called metabolites). Curve-fitting and interpolation techniques (*9*) were applied to blood and labeled metabolite time-activity curves. The tissue and blood curve data were then used to estimate thymidine influx into tissues, as described later.

FDG blood samples were centrifuged to separate plasma and red blood cells, and plasma was pipetted and counted to obtain FDG blood time-activity curves from time of injection to 60 min after injection. All blood and metabolite samples were counted on a Cobra well counter (Packard Instrument Co., Meriden, CT), which was cross-calibrated to the tomograph on the day of each study. Plasma glucose levels were measured at least three times over the course of the FDG study, and the average value was used in the metabolic rate of FDG (MRFDG) calculations.

In four patients, arterial blood sampling was performed during both the pre- and post-therapy scans. In one patient (Patient 6), venous blood sampling was performed during the pretherapy study for metabolite analysis, and total blood activity was determined from dynamic abdominal aorta images obtained as part of the imaging study. Aortic image data were corrected for partial-volume loss by comparison to late blood samples. In the post-therapy scan, total blood activity was determined from the abdominal aorta, but no blood sampling could be performed; so average metabolite curves obtained from a pool of previously studied patients were used (*9*). In one patient (Patient 4), blood samples were not

obtained and, because the patient's tumor was in the pelvis, there were no large blood vessels for determining total blood activity. In this patient, only standardized uptake value (SUV) determinations were made.

Thymidine uptake was quantified as follows:

$$SUV = \frac{\text{Average tissue activity } (\mu Ci/ml)}{(\text{Injected dose (mCi)/patient weight (kg)})}. \quad \text{Eq. 1}$$

The average tissue activity was calculated from ROI data from the images obtained 20–60 min after injection.

The thymidine blood-tissue transfer (flux) rate constant (K_{TdR}) was obtained from metabolite-corrected graphical analysis using blood and metabolite time-activity curves obtained 0–60 min after injection and the tissue time-activity curve obtained 20–60 min after injection (*8*). This flux value represents the steady-state flux of thymidine from the blood into tumor DNA (μmol/min/g tissue), as described by the following:

$$\text{Flux} = [TdR] \times K_{TdR}, \quad \text{Eq. 2}$$

where [TdR] is the concentration of native (unlabeled) thymidine in the plasma (μmol/ml) and K_{TdR} is the thymidine incorporation flux rate constant (ml/min/g). K_{TdR} is estimated graphically using a model that assumes thymidine is reversibly taken up into tissue and that some of the label is incorporated into DNA and therefore irreversibly bound in tissue over the time course of imaging. Because the native plasma level of thymidine was not measured, we used the rate constant as a measure of tumor proliferation and refer to this as the thymidine flux constant (K_{TdR}). The presence of labeled metabolites was considered using blood metabolite data with the assumption that none of the labeled metabolites were trapped in tissue to any significant extent (*8*). K_{TdR} reflects the steady-state rate of thymidine incorporation through the external or salvage pathway. This has been shown to be closely tied to the rate of DNA synthesis in the tumor (*17–19*).

FDG uptake was quantified as both SUV and metabolic rate. SUV was calculated using Equation 1. The average tissue activity was calculated from ROI data obtained 30–60 min after injection. This measurement reflects the accumulated activity of FDG in the tumor.

The FDG flux constant was estimated from the 0–60-min blood time-activity curve and the 20–60-min tissue time-activity curve using standard graphical analysis (*20,21*). Glucose metabolic rates were calculated by multiplying the flux constant × the plasma glucose concentration, obtained from measurements performed at the time of the study. No assumptions about a lumped constant were made so that the estimated metabolic rate is appropriately described as MRFDG, with units μmol/min/100 g.

RESULTS

Three of the four patients with small cell lung cancer had pathologic or clinical evidence of a response to therapy. Patient 1 died of sepsis 19 days after the start of treatment and, at autopsy, his tumor was >95% necrotic and fibrotic. The rapid pathologic response of his tumor was reflected in the decline in thymidine uptake and in the FDG uptake seen 7 days after therapy (Fig. 1, Table 1). Patient 2 had a clinically complete response to treatment on the basis of findings on CT scans. His response lasted for 6 mo, and he died of recurrent disease 12 mo after the start of treatment. Patient 3 achieved a partial response, but brain metastases developed 10 mo after the start of therapy, and he died 12 mo after beginning treatment. In each of these patients, there was a marked decrease in both thymidine SUV and K_{TdR} and FDG SUV and MRFDG (Table 1). Patient 4, with small cell lung cancer metastatic to the abdomen and pelvis, had no response to cisplatin and etoposide on the basis of findings on serial chest radiographs obtained 2 mo after the start of that therapy. In that patient, only thymidine imaging of a pelvic metastasis was done, and it demonstrated a decline in SUV of only 8%. K_{TdR} was not calculated because blood sampling could not be done during either pre- or post-therapy scans. This patient was subsequently treated with cyclophosphamide, doxorubicin and vincristine with a good response and had a stable partial remission for 9 mo after the start of his second-line chemotherapy. A third PET study performed approximately 2 wk after the change in chemotherapy showed a 27% drop in the thymidine SUV compared with the study performed after the initial chemotherapy. Brain metastases subsequently developed, and the patient died 13 mo after first starting therapy.

In the patient with a high-grade sarcoma in his thigh, there was marked decrease in tumor metabolism in response to chemotherapy. Within 6 days, K_{TdR} was 0 and MRFDG had decreased by 58%. This patient had five cycles of chemotherapy followed by resection of the thigh lesion and was found to have no viable tumor left. Mediastinoscopy was also performed to evaluate chest disease, and biopsy samples showed evidence of viable metastatic tumor despite the complete response of the primary tumor. Recurrent disease developed subsequently in this patient's central nervous system. He was treated with high-dose chemotherapy and died 20 mo after he was first treated. Another patient with abdominal sarcoma had a negligible change in thymidine measurements, whereas FDG SUV and MRFDG increased by 69% and 85%, respectively. Based on serial CT scans, his disease progressed during the first course of treatment. He refused further treatment and died of progressive disease.

SUV and K_{TdR} for thymidine were correlated with each other (linear regression correlation constant, $r = 0.63$; $n = 10$; $p = 0.05$), as were SUV and MRFDG ($r = 0.67$, $n = 10$, $p < 0.05$). Changes after therapy in SUV versus flux estimates were also correlated (thymidine: $r = 0.86$, $n = 5$, $p = 0.06$; FDG: $r = 0.96$; $n = 5$, $p < 0.01$). Changes in thymidine and FDG SUV with therapy were significantly correlated ($r = 0.94$, $n = 5$, $p < 0.05$); however, changes with therapy in K_{TdR} were not as well correlated with changes in MRFDG ($r = 0.62$, $n = 5$, $p > 0.20$). Thus, changes in simple uptake measures for FDG and thymidine, which are partly reflective of delivery and distribution of tracer, were correlated, whereas changes in the flux measurements for the two tracers, which are more reflective of specific metabolic pathways, were not.

DISCUSSION

PET gives the opportunity to measure tumor metabolism in vivo and follow metabolic changes in response to therapy. Currently, the response of tumors to therapy is assessed on the basis of physical examination and anatomically based imaging. This makes it difficult to assess the early response to chemotherapy and does not allow clinicians to make timely decisions to change therapy when tumors fail to respond. As a result, patients are frequently subjected to excessive normal tissue toxicity. Repeated measurements of tumor metabolism made on biopsy specimens have been used successfully to obtain early measures of response to therapy (*22,23*). Such biopsy studies are limited by the necessity to invasively sample the tumor to measure response and by the heterogeneity of the tumor. Metabolic imaging using PET has the potential to overcome the limitations of biopsy-based methods, and preliminary investigations of FDG use to measure response to therapy have been promising (*24–27*).

This investigation of 2-^{11}C-thymidine in this preliminary group of patients demonstrates the potential of labeled thymi-

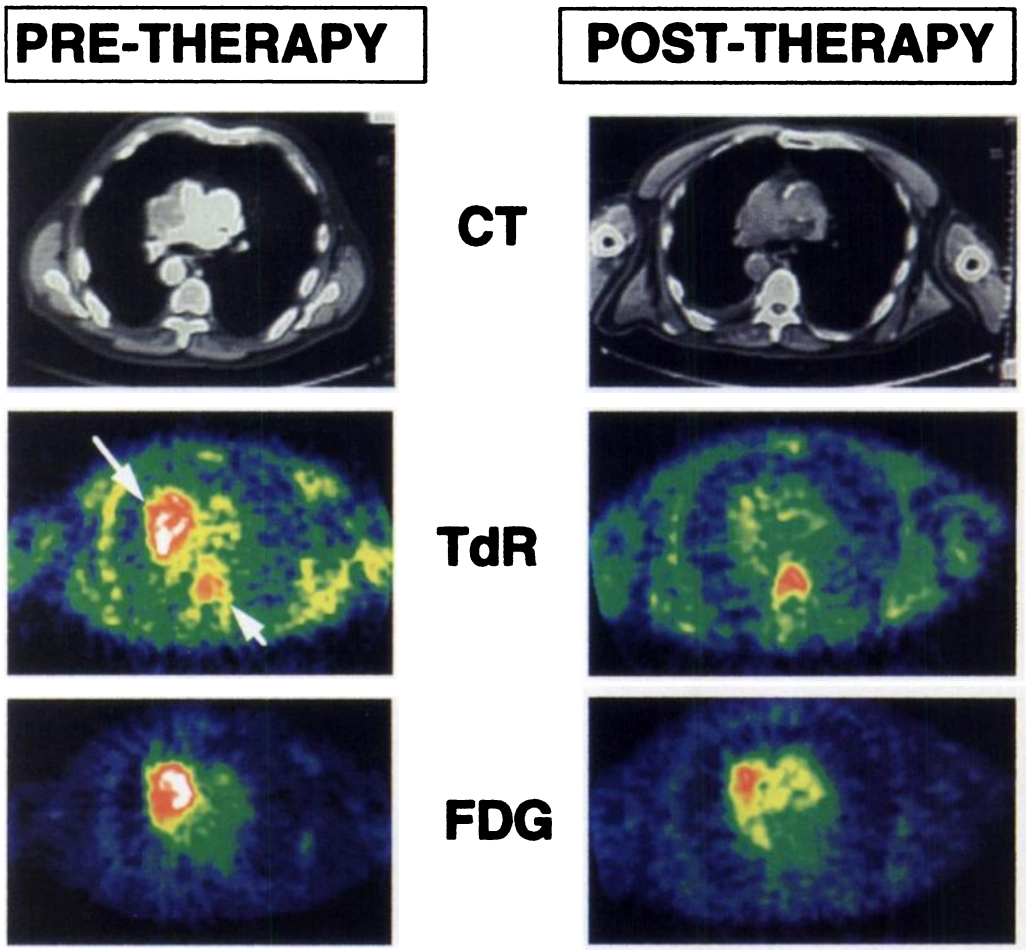

FIGURE 1. Images of small cell lung cancer (Patient 1). PET and CT images were obtained before and 6 days into therapy. Thymidine images were obtained 20–60 min postinjection, and FDG images obtained 30–60 min postinjection. Images of thymidine uptake show marked decline in tumor uptake (long arrow). Note thymidine uptake in vertebral marrow is visible before and after therapy (short arrow). Pretreatment CT scan was obtained with contrast medium, whereas post-treatment scan was obtained without contrast.

dine to provide accurate assessments of the early response to therapy. All four of the patients who responded to therapy showed significant declines in thymidine uptake early after therapy, whereas the two patients that did not respond to therapy showed no change or only minimal declines. In one of these patients, thymidine correctly identified a response when the patient was switched to chemotherapy, which ultimately proved to be initially successful in halting the progression of his disease. Although changes in FDG uptake in response to successful therapy were smaller than changes in thymidine uptake, FDG imaging was able to separate the four responders from the one nonresponder undergoing FDG imaging. These findings agree with in vitro studies of cellular response to therapy, in which measurements based on thymidine incorpo-

TABLE 1
Prechemotherapy Standardized Uptake Value (SUV) and Metabolic Rates and Percentage Decline with Therapy

			Thymidine						Fluorodeoxyglucose					
			SUV*			K_{TdR}			SUV			MRFDG*		
Disease	Patient no.	Response	Pre	Post	Decline† (%)	Pre	Post	Decline (%)	Pre	Post	Decline (%)	Pre	Post	Decline (%)
Lung cancer	1	Complete‡	2.9	0.9	69	0.115	0.000	100	6.7	3.2	52	20.7	13.9	33
	2	Complete	4.9	0.8	83	0.051	0.000	100	6.8	2.6	62	35.5	6.0	83
	3	Partial	1.8	0.9	48	0.063	0.041	35	4.9	2.5	50	24.5	5.3	79
	4§	Progressive	1.6	1.4	8	NA			NA			NA		
Sarcoma	5	Complete	3.3	1.5	55	0.102	0.000	100	13.1	7.9	40	28.5	12.1	58
	6	Progressive	1.4	1.3	3	0.020	0.017	15	2.6	4.4	−69	7.2	13.3	−85

*Measurements before chemotherapy included SUV, thymidine flux constant (K_{TdR}) and metabolic rate of FDG (MRFDG). Units for K_{TdR} are ml/min/g and for MRFDG are μmol/min/100 g.

†Percentage decline in indicated measurement after first cycle of therapy.

‡CR = complete response in the tumor as judged clinically.

§Patient 4 did not have blood sampling, so K_{TdR} could not be calculated. FDG was not done.

NA = not available.

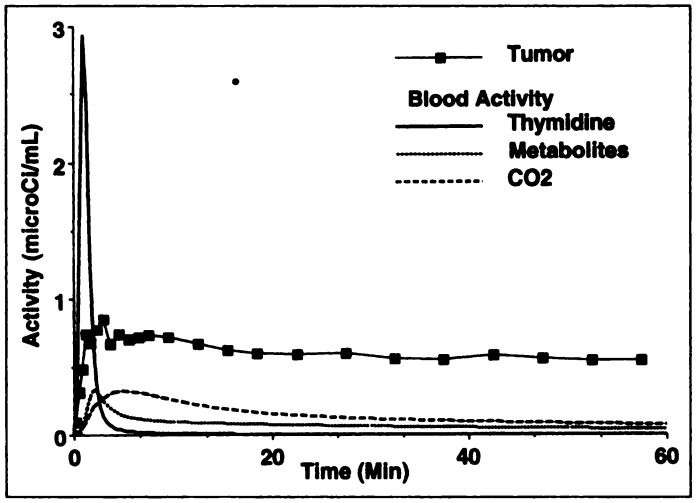

FIGURE 2. Blood and tumor time-activity curves. Graph demonstrates course of tumor activity before therapy, along with blood ^{11}C activity measured as thymidine, metabolites (primarily thymine and dihydrothymine) and bicarbonate. Data are from Patient 2. Blood activity has been fit using our modeling scheme.

ration and cellular energy metabolism were both able to measure cell death, but thymidine uptake declined more rapidly (*4*).

We found that SUV and flux measurements correlated with each tracer study. Although the changes in thymidine SUV and FDG SUV values with therapy were correlated, changes in the flux values were not correlated. Our explanation is that, with thymidine, minimum SUVs are close to 1 because of the contribution of labeled metabolites to the images, even when the corresponding flux was nearly 0. Labeled metabolites contribute to the simple uptake measurement but not to the flux parameter. This difference becomes important in interpreting post-therapy thymidine results, in which the estimation of K_{TdR} identified several tumors whose thymidine incorporation approached 0. In these patients, clinical and pathological follow-up suggested a complete response to therapy. In this limited series, thymidine flux measurements were able to show a shutdown in tumor proliferation in patients in whom FDG showed a more limited decrease in glucose metabolism. Further studies are needed to determine if these concepts will remain in a larger group of patients.

We studied only a limited number of patients undergoing chemotherapy for relatively high-grade tumors. Besides studying additional patients with similar tumor types, it will also be necessary to study patients with low-grade tumors, such as intermediate-grade sarcomas, to determine whether these tracers will perform equally well for less metabolically active tumors. Because lower-grade tumors often have a more variable response to chemotherapy, accurate early assessment of response may be even more important than in higher-grade tumors.

Besides the small number of patients, there are other limitations to this preliminary study. The ROI-based image analysis considered only the most active portion of relatively large tumors. Although it is likely that the most highly proliferative or metabolically active portion of the tumor will drive clinical decisions regarding therapy, analysis methods capable of assessing the heterogeneity of the tumor, both at baseline and in response to therapy, might provide a more accurate assessment of response. Furthermore, quantitative analysis considered only the overall flux of tracers from blood to tissue. More detailed compartmental analysis may provide more insight into the physiologic changes that occur when a tumor responds to chemotherapy.

CONCLUSION

PET imaging early after therapy demonstrated declines in thymidine and FDG retention within approximately 1 wk of successful chemotherapy. The changes in thymidine retention were greater, which suggests that it may be a more sensitive early indicator of tumor response to treatment. In the two patients with progressive disease, there was little change in thymidine retention. In most general oncology practices, the usual protocol is to give the patient approximately 2 mo of therapy and then repeat anatomic imaging, such as CT or MRI, to determine if the tumor is responding. If PET provides a more rapid assessment of response for other tumors and treatments, then it could help eliminate ineffective treatments after the first cycle of therapy. A PET scan costs less than most cycles of chemotherapy. Early assessment of response will help patients avoid the morbidity of ineffective treatment and allow them to receive other, potentially more effective treatments sooner.

ACKNOWLEDGMENTS

This work was supported in part by Grants CA 42045 and 39566 from the National Cancer Institute, by the Medical Research Service of the U.S. Department of Veterans Affairs and the Mallinckrodt Fellowship of the Society of Nuclear Medicine.

REFERENCES

1. Kubota R, Yamada S, Kubota K, Ishiwata K, Tamahashi N, Ido T. Intratumoral distribution of ^{18}F-fluorodeoxyglucose in vivo: high accumulation in macrophages and granulation tissues studied by microautoradiography. *J Nucl Med* 1992;33:1972–1980.
2. Shields AF, Larson SM, Grunbaum Z, Graham MM. Short-term thymidine uptake in normal and neoplastic tissues: studies for PET. *J Nucl Med* 1984;25:759–764.
3. Shields AF, Lim K, Grierson J, Link J, Krohn KA. Utilization of labeled thymidine in DNA synthesis: studies for PET. *J Nucl Med* 1990;31:337–342.
4. Kubota K, Ishiwata K, Kubota R, et al. Tracer feasibility for monitoring tumor radiotherapy: a quadruple tracer study with fluorine-18-fluorodeoxyglucose or fluorine-18-fluorodeoxyuridine, L-[methyl-^{14}C]methionine, [6-^{3}H]thymidine, and gallium-67. *J Nucl Med* 1991;32:2118–2123.
5. Sundoro-Wu BM, Schmall B, Conti PS, Dahl JR, Drumm P, Jacobsen JK. Selective alkylation of pyrimidyl-dianions: synthesis and purification of ^{11}C labeled thymidine for tumor visualization using positron emission tomography. *Int J Appl Radiat Isot* 1984;35:705–708.
6. Vander Borght T, Labar D, Pauwels S, Lambotte L. Production of [2-^{11}C]thymidine for quantification of cellular proliferation with PET. *Appl Radiat Isot* 1991;42:103–104.
7. Martiat P, Ferrant A, Labar D, et al. In vivo measurement of carbon-11 thymidine uptake in non-Hodgkin's lymphoma using positron emission tomography. *J Nucl Med* 1988;29:1633–1637.
8. Mankoff DA, Shields AF, Graham MM, Link JM, Krohn KA. A graphical analysis method for estimating blood-to-tissue transfer constants for tracers with labeled metabolites. *J Nucl Med* 1996;37:2049–2057.
9. Shields AF, Mankoff D, Graham MM, et al. Analysis of 2-Carbon-11-thymidine blood metabolites in PET imaging. *J Nucl Med* 1996;37:290–296.
10. Elias A, Ryan L, Sulkes A, Collins J, Aisner J, Antman K. Response to mesna, doxorubicin, ifosfamide, and dacarbazine in 108 patients with metastatic or unresectable sarcoma and no prior chemotherapy. *J Clin Oncol* 1989;7:1208–1216.
11. Link JM, Grierson JR, Krohn KA. Alternatives in the synthesis of 2-^{11}C-thymidine. *J Labelled Comp Radiopharm* 1995;37:610–611.
12. Hamacher K, Coenen HH, Stocklin G. Efficient stereospecific synthesis of no-carrier added 2-^{18}F--fluoro-2-deoxy-D-glucose using aminopolyether supported nucleophilic substitution. *J Nucl Med* 1986;27:235–238.
13. Lewellen TK, Bice AN, Miyaoka R, Harrison RL. Performance improvements for the SP-3000 time-of-flight positron emission tomograph. *J Nucl Med* 1990;31:863.
14. Lewellen TK, Miyaoka RS, Kohlmyer SG. Improving the performance of the SP 3000 PET detector modules. *IEEE Trans Nucl Sci* 1992;39:1074–1078.
15. Lewellen T, Kohlmyer S, Miyaoka R, Schubert S, Stearns C. Investigation of the count rate performance of the General Electric Advance positron emission tomograph. *IEEE Trans Nucl Sci* 1995;42:1051–1057.
16. DeGrado T, Turkington T, Williams J, Stearns C, Hoffman J. Performance characteristics of a whole-body PET scanner. *J Nucl Med* 1994;35:1398–1406.
17. Quackenbush RC, Shields AF. Local reutilization of thymidine in normal mouse tissues as measured with iododeoxyuridine. *Cell Tissue Kinet* 1988;21:381–387.
18. Cleaver JE. Thymidine metabolism and cell kinetics. *Front Biol* 1967;6:43–100.
19. Shields AF, Coonrod DV, Quackenbush RC, Crowley JJ. Cellular sources of thymidine nucleotides: studies for PET. *J Nucl Med* 1987;28:1435–1440.
20. Gjedde A. Calculation of cerebral glucose phosphorylation from brain uptake of glucose analogs in vivo: a reexamination. *Brain Res Rev* 1982;4:237–274.

21. Patlak CS, Blasberg RG, Fenstermacher JD. Graphical evaluation of blood-to-brain transfer constants from multiple-time uptake data. *J Cereb Blood Flow Metab* 1983;3:1–7.
22. Livingston RB, Sulkes A, Thirwell MP, Murphy WK, Hart JS. Cell kinetic parameters: Correlation with clinical response. In: Drewinko B, Humphrey RM, eds. *Growth kinetics and biochemical regulation of normal and malignant cells.* Baltimore: Williams and Wilkins; 1977:767–785.
23. Ensley JF. The clinical application of DNA content and kinetic parameters in the treatment of patients with squamous cell carcinomas of the head and neck. *Cancer Metastasis Rev* 1996;15:133–141.
24. Jansson T, Westlin JE, Ahlstrom H, Lilja A, Langstrom B, Bergh J. Positron emission tomography studies in patients with locally advanced and/or metastatic breast cancer: a method for early therapy evaluation? *J Clin Oncol* 1995;13:1470–1477.
25. Jones DN, Brizel DM, Charles HC, et al. Monitoring of response to neoadjuvant therapy of soft tissue and musculoskeletal sarcomas using ^{18}F-FDG PET [Abstract]. *J Nucl Med* 1994;35:38P.
26. Findlay M, Young H, Cunningham D, et al. Noninvasive monitoring of tumor metabolism using fluorodeoxyglucose and positron emission tomography in colorectal cancer liver metastases: correlation with tumor response to fluorouracil. *J Clin Oncol* 1996;14:700–708.
27. Shields AF, Graham MM, Spence AM. The role of PET imaging in clinical oncology: a current status report. *Nucl Med Ann* 1995a:129–168.

Tumor Cell Spheroids as a Model for Evaluation of Metabolic Changes After Irradiation

Reingard Senekowitsch-Schmidtke, Klaus Matzen, Regine Truckenbrodt, Johannes Mattes, Peter Heiss and Markus Schwaiger
Nuklearmedizinische Klinik und Poliklinik, Technische Universität München, Munich, Germany

Tumor cell spheroids provide a good model to evaluate the relationship between tumor volume and the number of viable cells in the volume with the uptake of metabolic tracers before and after therapy. They represent the only in vitro model that allows the determination of the activity per unit volume, a parameter which is relevant for interpretation of PET studies. The purpose of this study was to evaluate this model with respect to the uptake of ^{14}C-FDG, ^{3}H-methionine and ^{3}H-thymidine with and without exposure to irradiation. **Methods:** Spheroids of the human adenocarcinoma cell line SW 707 were incubated in media containing ^{14}C-FDG, ^{3}H-methionine or ^{3}H-thymidine for 1 hr at 1, 4, 8, 24 and 48 hr after exposure to a single radiation dose of 6 Gy together with control spheroids. Tracer uptake after incubation was expressed in cpm/spheroid, cpm/1000 viable cells and cpm/0.01 mm^3. In addition, the proliferative capacity of control and irradiated spheroids was determined using the clonogenic assay. **Results:** Spheroid uptake of FDG decreased with time after irradiation, while the uptake per 1000 viable cells was increased significantly. The activity per unit volume remained unchanged in comparison to control spheroids. Methionine uptake per spheroid was unchanged after irradiation because of the high increase in uptake per 1000 viable cells. Uptake per unit volume also remained unchanged in comparison to controls. Thymidine uptake per 1000 viable cells did not change after irradiation but showed significant differences in uptake per spheroid and per unit volume compared to controls. The percentage of thymidine incorporated into the TCA-precipitable fraction containing DNA was 50% in controls and decreased to 12% at 24 hr after irradiation. The suppressed clonogenic capacity early after therapy recovered with the increase in thymidine uptake and with the increase in thymidine incorporation into DNA. **Conclusion:** The results show that the activity determined within a certain tumor volume is a balance between the increased tracer uptake by surviving cells after therapy and the lack of tracer uptake by dead cells, which still contribute to the tumor volume. Thus, the resulting unchanged activity per unit volume within the spheroid, as found for FDG and methionine, may not fully reflect therapy-induced metabolic changes in tumors.

Key Words: tumor cell spheroids; therapy monitoring; fluorodeoxyglucose; nucleotide and amino acid uptake; PET tumor tracers

J Nucl Med 1998; 39:1762–1768

The use of radiolabeled 2-fluoro-2-deoxy-D-glucose (FDG), thymidine and amino acids in PET studies has been applied increasingly to assess tumor response to different therapy regimens through alteration in tumor metabolism. In addition to ^{18}F-FDG, other tracers, especially ^{11}C-L-methionine, have been used for PET studies since labeling of this amino acid with ^{11}C is relatively uncomplicated for routine production. While ^{18}F-FDG and ^{11}C-methionine uptakes reflect metabolic activity, the uptake of the nucleotide precursor, ^{11}C-thymidine, is considered a measure of proliferative activity.

Many clinical studies have demonstrated that a reduction of ^{18}F-FDG or ^{11}C-methionine uptake after therapy, as determined by PET, correlates to positive clinical results obtained by other methods. Experimental studies with transplanted tumors also demonstrated a rapid decrease in tumor uptake of ^{3}H-thymidine, ^{3}H-methionine and ^{18}F- or ^{14}C-FDG after irradiation, which preceded a change in tumor volume (*1–6*). However, the interpretation of the PET signal after therapy is still unclear. In some cases, tumor uptake remained at the pretreatment level or even increased after radiotherapy, despite a reduction in tumor mass. Although inflammatory tumor reactions with high metabolic activity in invading macrophages and granulocytes have been suggested to explain this phenomenon (*7*), in vitro studies with cultured human tumor cells also have shown a significant increase in uptake of metabolic tracers in the surviving tumor cells after irradiation or treatment with cytostatic drugs (*8–12*). Thus, it is important to investigate the relationship between tumor volume or number of viable cells and the uptake of FDG, thymidine and methionine, with and without exposure to irradiation, in a three-dimensional tumor model.

Multicellular tumor spheroids have several biologic characteristics in common with in vivo tumors. These three-dimensional cell aggregates represent models intermediate in complexity between two-dimensional monolayer cultures in vitro and transplanted tumors in vivo (*13–15*). Tumor spheroids with a diameter of 350 μm consist of approximately 12,000 cells, which allow penetration of tracers to the spheroid center within several minutes (*16,17*).

Similar to in vivo tumors, tumor spheroids are composed of cells with different metabolic activity and, consequently, with variable uptake of metabolic tracers. Since PET visualizes the mean uptake per unit volume in a tumor composed of cells of higher and lower metabolic activities as well as necrotic cells,

Received Aug. 13, 1997; revision accepted Jan. 12, 1998.
For correspondence or reprints contact: Reingard Senekowitsch-Schmidtke, MD, PhD, Nuklearmedizinische Klinik und Poliklinik der Technischen Universität München, Ismaningerstr. 22, 81675 Munich, Germany.